Wave failure at strong coupling in intracellular Ca^{2+} signaling system with clustered channels

Xiang Li,[1,2] Yuning Wu,[1] Xuejuan Gao,[1] Meichun Cai,[1] and Jianwei Shuai[1,2,3,*]

[1]*Department of Physics, Xiamen University, Xiamen 361005, China*

[2]*State Key Laboratory of Cellular Stress Biology, Innovation Center for Cell Signaling Network, Xiamen University, Xiamen 361102, China*

[3]*Research Institute for Biomimetics and Soft Matter, Fujian Provincial Key Laboratory for Soft Functional Materials Research, Xiamen University, Xiamen 361102, China*

(Received 15 August 2017; published 17 January 2018)

As an important intracellular signal, Ca^{2+} ions control diverse cellular functions. In this paper, we discuss the Ca^{2+} signaling with a two-dimensional model in which the inositol 1,4,5-trisphosphate (IP_3) receptor channels are distributed in clusters on the endoplasmic reticulum membrane. The wave failure at large Ca^{2+} diffusion coupling is discussed in detail in the model. We show that with varying model parameters the wave failure is a robust behavior with either deterministic or stochastic channel dynamics. We suggest that the wave failure should be a general behavior in inhomogeneous diffusing systems with clustered excitable regions and may occur in biological Ca^{2+} signaling systems.

DOI: 10.1103/PhysRevE.97.012406

I. INTRODUCTION

As an important second intracellular messenger in living cells, calcium signals (Ca^{2+}) encode the stimulus, such as inositol 1,4,5-trisphosphate (IP_3), and control a wide array of cellular functions, including egg activation, muscle contraction, motility, learning and memory, gene expression, metabolic processes, and cell differentiation and apoptosis [1,2]. Intracellular Ca^{2+} waves have been first observed in medaka eggs [3] and later on in many different types of cells [4–8]. Intracellular Ca^{2+} ions are released from internal Ca^{2+} stores, most notably the endoplasmic reticulum (ER) or sarcoplasmic reticulum (SR), through inositol 1,4,5-trisphosphate receptor channels (IP_3R) or ryanodine receptors (RyR) [9,10]. Experiments have revealed that the IP_3Rs or RyRs are distributed in clusters as active regions, spaced a few micrometers apart and with several or a few tens of channels per cluster. The localized Ca^{2+} liberations at discrete excitable sites are termed as puffs or sparks [6,8,10–12]. Local Ca^{2+} release events can merge to form global release events in the form of Ca^{2+} oscillations and waves [6].

The inhomogeneous excitability of Ca^{2+} signaling system has attracted many numerical simulations [13,14]. For the localized Ca^{2+} puffs, the IP_3R channels showed strong stochastic open and closing dynamics [15]. The clustering of a few tens of IP_3Rs could increase the coherent Ca^{2+} puffs to respond to the weak IP_3 stimulation [16]. Because of the sharp decay of Ca^{2+} concentration around the open channels, two scales of Ca^{2+} concentrations have been suggested to describe the values for open channels and closed channels, respectively, leading to a breakdown of detailed balance on the coarse-grained level of puff models [17]. By discussing the interpuff intervals of a diffusing Ca^{2+} model, a division of tasks between global feedbacks and local cluster properties have been revealed to guarantee robustness of function while maintaining sensitivity of control of the average interpuff interval [18]. More recently, it has been shown that the synchronization corresponding to termination of local Ca^{2+} signals that are generated by clustered Ca^{2+} channels can be described by the phase transition associated with the reversal of magnetic field in a classical Ising ferromagnet [19].

Besides the discussion on puff dynamics, the transition mechanisms from puffs to waves have also been discussed numerically. With a stochastic version of the fire-diffuse-fire threshold model [20], it has been shown that stochastic calcium release leads to the spontaneous production of calcium puffs that may merge to form abortive or saltatory waves [20], and the phase transition between propagating and abortive waves is the same as for models in the directed percolation universality class [21]. The lifetime difference between short puffs and long-period waves can be partly understood with strongly reduced ordinary differential equations modified by a time-scale factor that takes into account the coupling strength of active and passive regions determined by the Ca^{2+} diffusion coefficient [22]. Later, it has been suggested that the different lifetimes of puffs and waves are determined by their different termination dynamics that puffs are terminated by Ca^{2+} inhibition while IP_3 unbinding is responsible for termination of waves [23]. The puff releases are sensitive to the strength of IP_3 stimulation and the residual Ca^{2+} concentration around cluster domain, while with high IP_3 concentration global waves are built up by long-sustained Ca^{2+} release events with synchronous unbinding and rebinding of IP_3 to channels [24]. The transition from stochastic sparks to Ca^{2+} travelling waves in ventricular myocytes through cluste red RyRs is also simulated and discussed [25].

The global Ca^{2+} oscillations with the propagating waves have been attracted much attention also, because the Ca^{2+} signal is mainly carried by the frequency of Ca^{2+} oscillation. It has been shown that the spatially nonuniform media can generate various spatially Ca^{2+} signals, including localized

*jianweishuai@xmu.edu.cn

puffs, stochastic backfiring, abortive waves, spiral waves, and globally salutatory or continuous waves [20,26–28]. With inhomogeneous media, the cell's capability of creating a globally periodic Ca^{2+} response to weak IP_3 stimulation can also be enhanced [29]. By replenishing the Ca^{2+} load of the cell, the membrane transport for Ca^{2+} can control the intracellular Ca^{2+} oscillations [30]. It has been pointed out that the channel stochasticity can destroy the global Ca^{2+} oscillation, but the additional small global fluctuations in IP_3 can partially restore temporal and spatial coherence of the oscillatory Ca^{2+} signal [31]. A common dynamical structure was suggested underlying Ca^{2+} oscillations of widely varying period that occur at constant IP_3 concentration in different cell types [19].

From these numerical studies, one may conclude that cluster-distributed excitability of Ca^{2+} release dynamics provides the cell with a flexible signaling repertoire for intracellular information transportation. It has been shown that the wave propagation can become abortive in inhomogeneous system [20,21,32,33]. Bressloff indicated that propagation failure can occur in an inhomogeneous excitable neural medium if the wave speed is too slow or the degree of inhomogeneity is too large [32]. A periodic modulation of the long-range connections in excitatory neural network can slow down the propagating wave, and the wave propagation failure can occur if the amplitude and wavelength of the periodic modulation is sufficiently large [33]. More interestingly, Pando *et al.* discussed Ca^{2+} ions diffuse in two-dimensional space with the fire-diffuse-fire model [34]. They found that the Ca^{2+} waves undergo propagation failure with increasing diffusion coefficient. This is because strong Ca^{2+} diffusion plays a dual role here, which is necessary for wave propagation but also acts as a sink to remove Ca^{2+} ions from the ER membrane. Waves in homogeneous media do not share such a counterintuitive property. The Ca^{2+} fire-diffuse-fire model was developed as an abstract model to capture only the dynamics of Ca^{2+}-induced-Ca^{2+}-release. So, the model does not take into account the complexities of channel gating dynamics, and the Ca^{2+} is released from point sources in one-dimensional membrane [34].

By now the phenomenon of wave failure has recieved little attention in literature, and it remains unclear if such an interesting behavior can occur in biological Ca^{2+} signaling system. In this paper, we discuss the Ca^{2+} wave failure with a more biologically realistic model. In the model, the channel clusters have a biological size of 500 nm and are distributed in a regular array of two-dimensional regions. The open and closing kinetics of channels are described with deterministic or stochastic dynamics by considering the binding and unbinding of Ca^{2+} and IP_3 messengers to the receptor in detail. We show that the wave failure can be observed with varying model parameters and with either deterministic or stochastic channel dynamics. The robustness of wave failure indicates that such a behavior should be a general phenomenon in inhomogeneous system with a lattice of active regions and may occur in biological Ca^{2+} signaling systems.

II. INTRACELLULAR Ca^{2+} DIFFUSION MODEL

We model the cytosolic space as a two-dimensional sheet, in which the Ca^{2+} concentration $C(x,y,t)$ is described by the following reaction diffusion equation:

$$\frac{\partial C}{\partial t} = D\nabla^2 C + f(x,y)J_C - J_P + J_L, \tag{1}$$

where C denotes Ca^{2+} concentration, D the Ca^{2+} diffusion coefficient, J_C the Ca^{2+} flux from ER to the cytosol through clustered IP_3Rs, J_P the SERCA pump flux from the cytosol to ER, and J_L the leakage flux from ER to the cytosol. The pump and leakage are homogeneously distributed over the ER membrane, while the IP_3Rs are distribute in clusters positioned on a regular lattice and described by the following function $f(x,y)$:

$$f(x,y) = \sum_i \sum_j \left(\Theta\left(x - iL - \frac{l}{2}\right) - \Theta\left(x - iL + \frac{l}{2}\right)\right) \times \left(\Theta\left(y - jL - \frac{l}{2}\right) - \Theta\left(y - jL + \frac{l}{2}\right)\right), \tag{2}$$

with the Heaviside function $\Theta(x) = 0$ for $x < 0$, otherwise, 1. As a result, the function $f(x,y) = 1$ at the active regions with channels; otherwise, $f(x,y) = 0$ for passive region. Accordingly, each channel patch is a square active region with a side length of l, and the most nearby channel patches have a distance of L.

The three fluxes in Eq. (1) are given by

$$J_C = v_C m_\infty^3 n_\infty^3 h^3 (C_{ER} - C), \tag{3}$$

$$J_P = v_P \frac{C^2}{k^2 + C^2}, \tag{4}$$

$$J_L = v_L (C_{ER} - C), \tag{5}$$

in which C_{ER} describes the Ca^{2+} concentration in ER. The parameters v_C, v_P, and v_L describe the maximum flux through a cluster of IP_3Rs, maximum pump flux, and leakage rate, respectively.

The flux J_C through a cluster of channels is determined by the fraction of open IP_3Rs in the cluster. Various kinetic models have been proposed to study IP_3R gating dynamics [35–40]. In the paper, we apply the Li-Rinzel model [35] to describe channel dynamics, which is a simplification of the DeYoung-Keizer model [36]. Each channel has three identical and independent subunits. Each subunit has a binding site for IP_3 (i.e., m gate) and two binding sites for Ca^{2+}, one for activation (i.e., n gate), and one for inactivation (i.e., h gate). The subunit becomes active only when IP_3 and activating Ca^{2+} sites are both bound. The channel is open if all three subunits are in active state. In Li-Rinzel model, binding probabilities of IP_3 and activating Ca^{2+} are instantaneous and represented by their quasisteady states $m_\infty = p/(p + d_m)$ and $n_\infty = C/(C + d_n)$ with p the IP_3 concentration. The Ca^{2+}-inactivation h gate is slow and described by

$$\frac{dh}{dt} = \alpha(1 - h) - \beta h, \tag{6}$$

with the binding and dissociation rates $\alpha = a_1(p + d_1)/(p + d_2)$ and $\beta = a_2 C$.

In the simulation, an area of $60\,\mu m \times 60\,\mu m$ membrane is considered with most nearby cluster distance

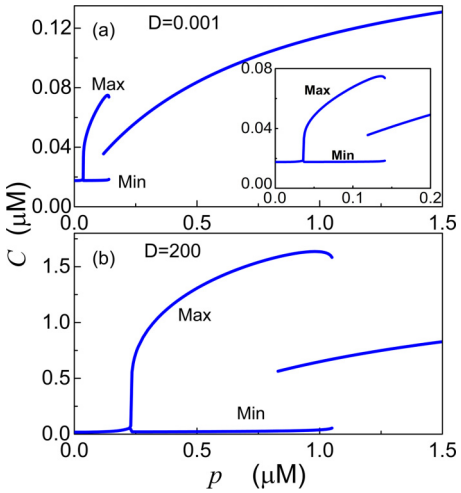

FIG. 1. Bifurcation diagrams of two-dimensional Ca^{2+} diffusion model, i.e., the maximal and minimal concentrations of $\langle C\rangle$, against p at $D = 0.001\,\mu m^2/s$ (a) and at $D = 200\,\mu m^2/s$ (b). The inset in (a) is an enlarged part for p in the range of $(0, 0.2\,\mu m)$.

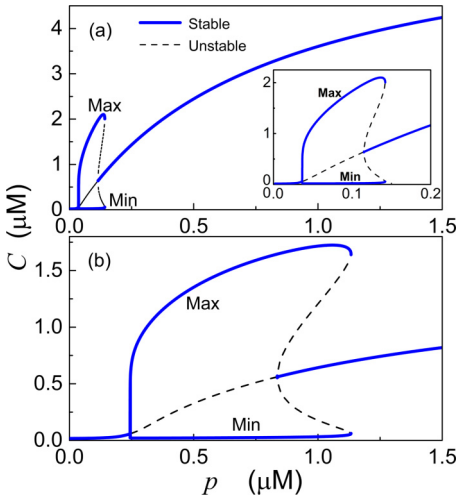

FIG. 2. Bifurcation diagrams of C against p for the point models with Eqs. (6) and (7) (a) and with Eqs. (6) and (8) (b). The inset in (a) is the enlarged part for p in the range between 0 and $0.2\,\mu M$. Solid lines are for stable states and dashed lines for unstable states.

$L = 3\,\mu m$ and cluster size $l = 0.5\,\mu m$. Non-flux boundary condition is applied in the model. The parameters in the IP_3R model are given as follows: $v_C = 21.6/s$, $v_P = 0.5/s$, $v_L = 0.001\,\mu M/s$, $C_{ER} = 15\,\mu M$, $k = 0.1\,\mu M$, $d_m = 0.13\,\mu M$, $d_n = 0.08\,\mu M$, $a_1 = 0.21/s$, $a_2 = 0.2/\mu M/s$, $d_1 = 0.13\,\mu M$, and $d_2 = 0.94\,\mu M$ [31].

In the simulation, the Eular method (i.e., the first-order numerical procedure) is used for solving Eq. (1) with the grid-size dx equalling to the cluster size l for simplicity and the time step dt typically 0.2 ms [28]. Our simulation results indicate that with smaller grid-size (such as $dx = l/2$), the similar bifurcation results can still be obtained.

III. SIMULATION RESULTS

A. The point model approximation at very small or large D

To discuss how the diffusion coefficient D modulates the Ca^{2+} release dynamics, we first consider the two extreme cases of the Ca^{2+} diffusion model, i.e., at very small and large D. The bifurcation diagrams of the cell averaged Ca^{2+} concentration $\langle C\rangle$, i.e., the maximal and minimal concentrations of $\langle C\rangle$, against IP_3 concentration p are plotted at $D = 0.001$ and $200\,\mu m^2/s$ in Figs. 1(a) and 1(b), respectively. One can see that an oscillation is found in the small region of $0.037 < p < 0.141\,\mu M$ at $D = 0.001\,\mu m^2/s$, and in the large region of $0.23 < p < 1.04\,\mu M$ at $D = 200\,\mu m^2/s$.

Actually, such bifurcation behaviors of the two-dimensional Ca^{2+} diffusion model at very small and large D can be well understood with the simple point model [22]. For small D, all the regions can be treated as independent domains. With $D \to 0$, the oscillation dynamics of the cell averaged Ca^{2+} concentration can be explained by the Ca^{2+} dynamics in the active region, which is described by

$$\frac{dC}{dt} = J_C - J_P + J_L, \tag{7}$$

with the equation for h given by Eq. (6).

However, at large D the coupling is so strong that all the active and passive regions experience almost the same calcium concentration, giving $\nabla^2 C \to 0$ for the system. The fact of $\nabla^2 C \to 0$ indicates that the released Ca^{2+} ions from active regions have to be shared by both active and passive regions. Thus, the Ca^{2+} dynamics can be described by the following equation [22],

$$\frac{dC}{dt} = \lambda \times J_C - J_P + J_L, \tag{8}$$

with the rescale factor λ representing the averaging effect of the released Ca^{2+} ions by both active and passive regions, given by

$$\lambda = \frac{S_{\text{Active}}}{S_{\text{Active}} + S_{\text{Passive}}} = \frac{l^2}{L^2}, \tag{9}$$

where S_{Active} and S_{Passive} are the areas of the active and passive regions, respectively. Here we have $\lambda = 0.027$ with $l = 0.5\,\mu m$ and $L = 3\,\mu m$.

For the point model, the bifurcation diagrams, i.e., the maximal and minimal C, against p are plotted in Figs. 2(a) and 2(b) with Eqs. (6) and (7) and Eqs. (6) and (8), respectively. Through Hopf bifurcation, an oscillation region occurs at middle p, with the stable and unstable states denoted by solid and dashed lines, respectively, in Fig. 2. The oscillating dynamics can be found for p in the range of 0.036 and 0.142 with Eqs. (6) and (7), and in the range of 0.24 and 1.13 with Eqs. (6) and (8), respectively.

As a result, the Ca^{2+} bifurcations of the Ca^{2+} diffusion model at large and small D can be well understood with the point model. For the point model, with the decrease of λ from 1 to 1/37, simulation results show that the oscillation range in bifurcation diagrams against p simply keeps enlarged with the left bifurcation point shifting from 0.04 to 0.23. Quite differently, the Ca^{2+} diffusion model exhibits rich bifurcation behaviors with varying D, as shown in the following sections.

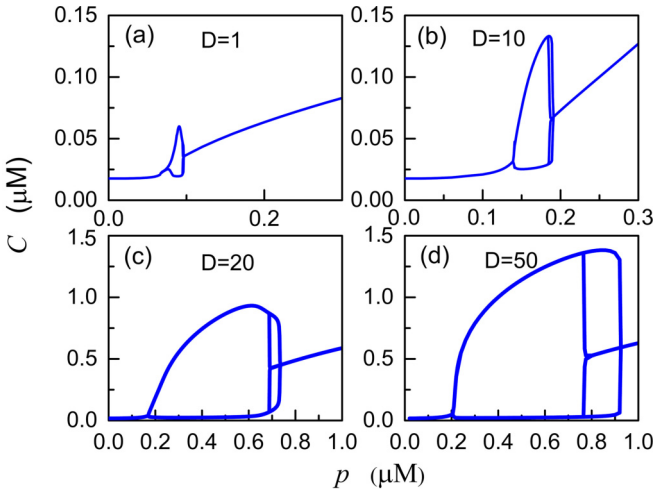

FIG. 3. Bifurcation diagrams of $\langle C\rangle$ against p for the Ca^{2+} diffusion model at different D. In (a)–(d), $D = 1$, 10, 20, and 50 $\mu m^2/s$, respectively.

B. Ca^{2+} bifurcation diagrams against p at different D

Now we discuss how the diffusion coefficient D modulates the Ca^{2+} release dynamics in Ca^{2+} diffusion model. The bifurcation diagrams of cell-averaged $\langle C\rangle$ against p are plotted in Figs. 3 and 4 with different D. Figure 3 plots the bifurcation diagrams of $\langle C\rangle$ against p with $D = 1$, 10, 20, and 50 $\mu m^2/s$, showing an enlarged oscillation region in p with increasing D as predicted by the point model.

However, Fig. 4 indicates that complex oscillation dynamics can be observed in the Ca^{2+} diffusion model with D changing in a narrow range between 12 and 15 $\mu m^2/s$. Interestingly, Fig. 4(a) shows that an additional oscillating region (i.e., A1) occurs around $p = 0.5\,\mu M$ at $D = 12\,\mu m^2/s$, giving two oscillation regions (i.e., A1 and A2) with the increasing p. With the further increase of D, the ranges of the two oscillating

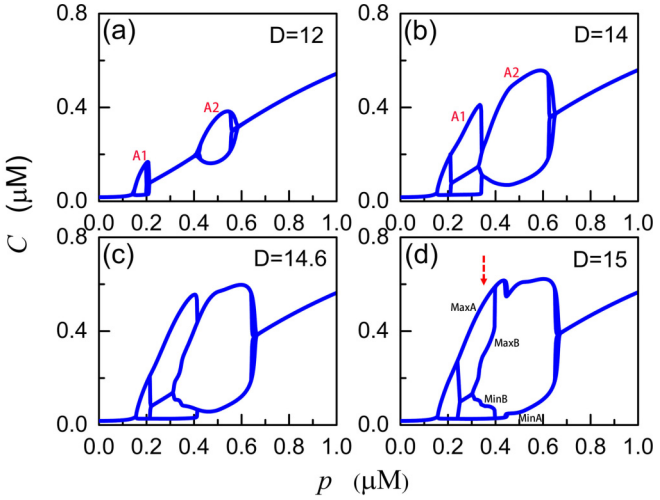

FIG. 4. The bifurcation diagrams of $\langle C\rangle$ against p for the Ca^{2+} diffusion model at different D. In (a)–(d), $D = 12$, 14, 14.6, and 15 $\mu m^2/s$, respectively.

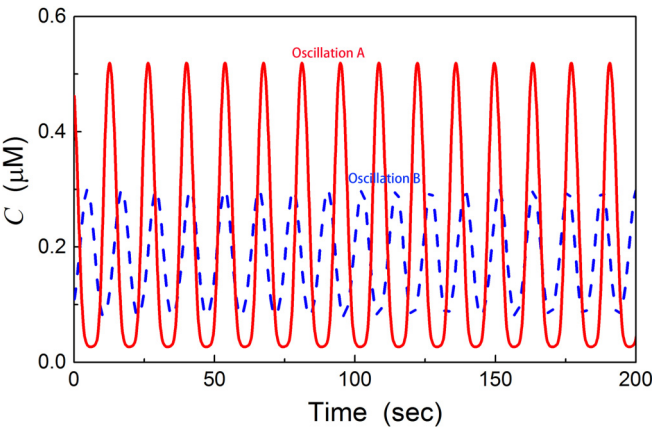

FIG. 5. The trajectories $\langle C\rangle$ of bistable oscillation states of the Ca^{2+} diffusion model at $D = 15\,\mu m^2/s$ and $p = 0.35\,\mu M$.

regions in p both become enlarged, and the corresponding oscillating amplitudes increase also. Around $D = 14\,\mu m^2/s$, the two oscillating regions A1 and A2 become overlapping and merge into a large oscillating region [Fig. 4(b)].

Within the oscillating region, one can observe a single stable oscillation state or bistable states. The bistable states can be either an oscillation state with a fixed piont, or two oscillation states with different oscillating amplitudes and frequencies (Figs. 4(c) and 4(d)]. As shown in Fig. 4(d), for the bistable oscillation states, their maximal and minimal amplitudes are marked as MaxA and MinA, and MaxB and MinB, respectively. At $p = 0.21\,\mu M$ and $D = 15\,\mu m^2/s$, which is labeled with a red arrow, the corresponding two oscillation trajectories of $\langle C\rangle$ are plotted in Fig. 5 with a red line for oscillation A and a blue dashed line for oscillation B.

C. Ca^{2+} bifurcation diagrams against D at different p

Next, we discuss the bifurcation diagrams of $\langle C\rangle$ against D of the Ca^{2+} diffusion model. With $0.25 \leqslant p \leqslant 1.1\,\mu M$, the Ca^{2+} diffusion model shows Ca^{2+} waves at large D, but does not exhibit any oscillation at small D. As an example, the bifurcation diagram of $\langle C\rangle$ against D is given in Fig. 6(a) at $p = 0.3\,\mu M$. The propagation waves are always observed at large D.

As shown in Figs. 6(b) and 6(c), an interesting observation is found for p at 0.2 and 0.1 μM. The bifurcation diagrams indicate that the propagating waves occur only at limited range of D. In other words, the Ca^{2+} diffusion system does not exhibit any oscillation not only at small D, but also at large D. The behavior that the Ca^{2+} waves undergo wave failure at large D could not occur in homogeneous media [19]. In our model, the 2D media consists of a lattice Ca^{2+} channel clusters distributed on the passive ER membrane. The oscillation frequency of propagation waves against D is plotted in Fig. 6(d). With the increasing D, the oscillation frequency typically keeps decreasing.

As plotted in Fig. 6(b) at $p = 0.2\,\mu M$, with small D, each excitable region can be treated as an independent Ca^{2+} system, giving no oscillation. With coupling in $11.1 \leqslant D \leqslant 43.0\,\mu m^2/s$, the proper interaction between pump dynamics in the passive region and the channel dynamics in the excitable

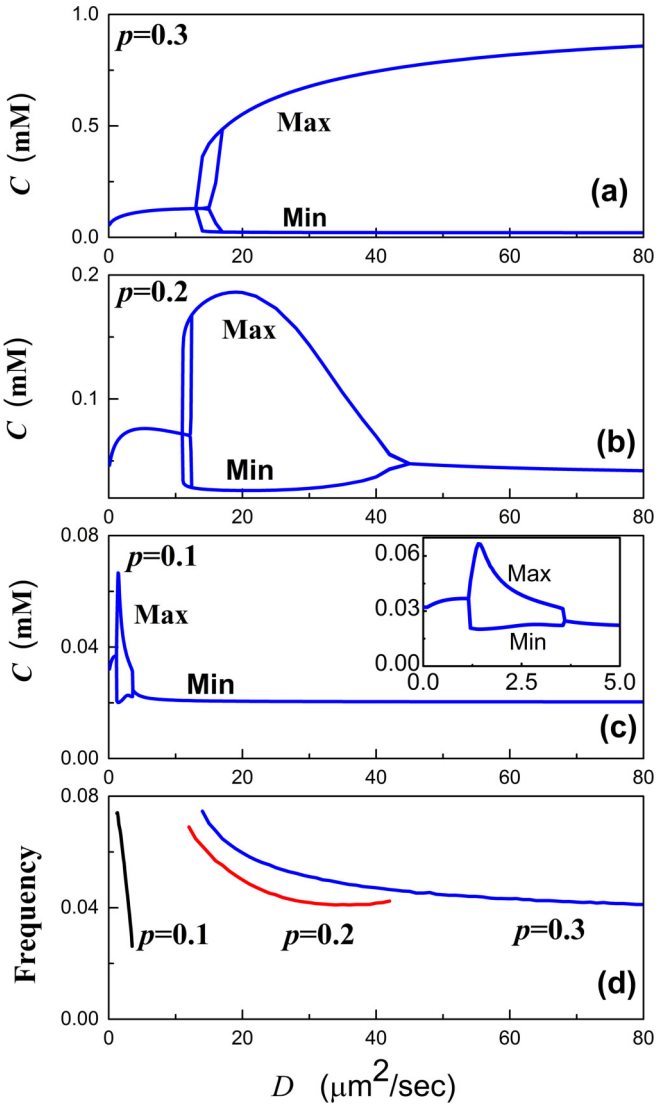

FIG. 6. (a)–(c) Bifurcation diagrams of $\langle C\rangle$ against D for the Ca^{2+} diffusion model at $p = 0.3$, 0.2, and 0.1 μM, respectively. The inset in (c) is the enlarged part for D in the range of (0, 5 $\mu m^2/s$). (d) The oscillation frequency of Ca^{2+} wave against D at $p = 0.3$ (blue line), 0.2 (red line), and 0.1 μM (black line).

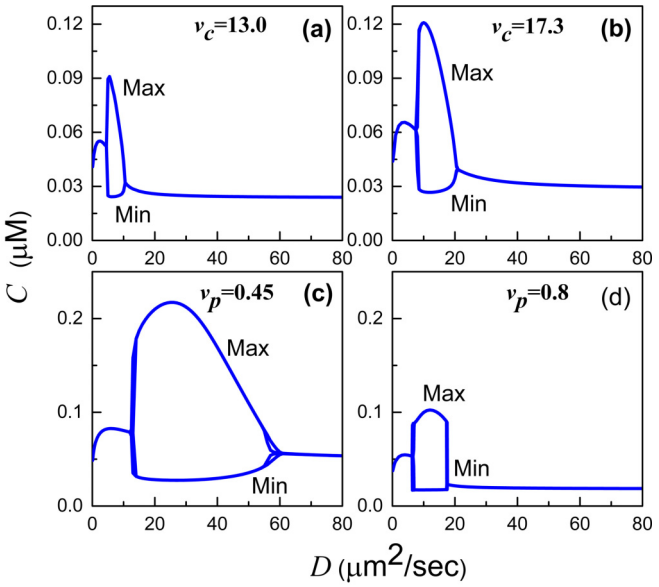

FIG. 7. Robustness of wave failure with varying model parameters. Bifurcation diagrams of $\langle C\rangle$ against D for the Ca^{2+} diffusion model at different maximum channel flux with $v_C = 13.0$ (a) and 17.3 s^{-1} (b) and different maximum pump flux with $v_P = 0.45$ (c) and 0.8 s^{-1} (d), respectively.

regions generates global Ca^{2+} wave propagations. However, with $D > 43.0\,\mu m^2/s$, the strong Ca^{2+} diffusion dynamics can largely remove Ca^{2+} ions from the active regions, causing the wave failure.

In the model the two important terms for Ca^{2+} oscillation are channel dynamics in active regions and pump dynamics on the ER membrane. A proper interaction between the release dynamics of Ca^{2+} channels and the sink dynamics of Ca^{2+} pump is necessary to support wave propagation. Now we discuss the robustness of the wave failure with varying model parameters of these two important terms. The bifurcation diagrams are given in Figs. 7(a) and 7(b) with the maximum channel flux decreasing from $v_C = 21.6/s$ to its 80% and 60%, and in Figs. 7(c) and 7(d) with the maximum pump flux v_P changing from $v_P = 0.5/s$ to 0.45 and 0.8/s, respectively. Our simulation results indicate that by changing the maximum channel or pump flux in a certain range, one can still observe the wave failure.

D. Wave failure with stochastic channel dynamics

The clustered channels show a strong stochastic behavior in the realistic Ca^{2+} signaling system due to the thermal opening and closing of the individual channels in each cluster with a small number of channels [15]. The channel fluxes with stochastic channel dynamics can be expressed as

$$J_{\text{Channel}} = v_C m_\infty^3 n_\infty^3 \frac{N_{h-\text{open}}}{N}(C_{\text{ER}} - C), \tag{10}$$

where $N_{h-\text{open}}$ denotes the number of noninhibited channels in the cluster. In the simulation, a Markov process is applied to perform the stochastic gating dynamics [15]. In detail, the state of each channel is updated for every small time step dt. Each IP_3R channel has three two-state h gates, i.e., h-open or h-closed, which is Ca^{2+} unbound or bound at the inhibited binding site, respectively. If an h gate is closed at time t, then the probability that it remains closed at time $t + dt$ is αdt, and if it is open at time t, then the probability that it remains open at time $t + dt$ is βdt. To determine the state of a gate, random numbers are drawn consistent with these probabilities. Only if all three h gates in an IP_3R channel are open at time t, the channel is h-disinactivated or h-open, contributing a unit to $N_{\text{h-open}}$ [15].

Considering 36 IP_3Rs in each cluster, we apply the Markov simulations for channels to investigate the stochastic spatiotemporal Ca^{2+} waves. As an example, a series of snapshots of stochastic propagation wave are shown in Fig. 8 at $p = 0.5\,\mu$M and $D = 15\,\mu m^2/s$. A mean period of about 12 s is observed for the noisy oscillation.

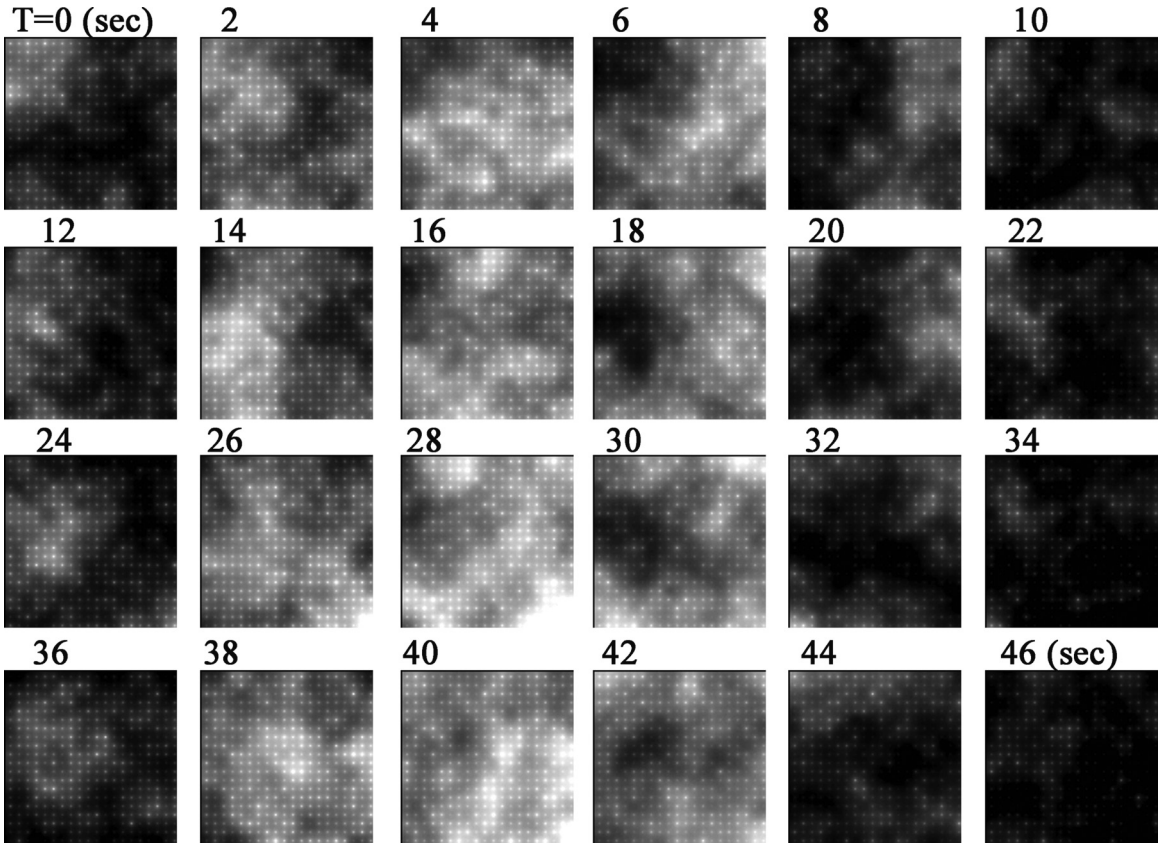

FIG. 8. The snapshots of stochastic propagation wave at $p = 0.5\,\mu$M and $D = 15\,\mu\text{m}^2/\text{s}$. The time interval is 2 s between two successive snapshots.

By calculating the averaged maximum and minimum of concentration $\langle C\rangle$ for certain time intervals, one can still discuss the bifurcation diagram of the stochastic propagation model. In detail, we calculate the averaged maximum and minimum over 50 times with each time interval of 100 s, giving variance typically smaller than 0.005. Figure 9 plots the bifurcation diagrams of $\langle C\rangle$ against p at $D = 10$, 15, 20, and $50\,\mu\text{m}^2/\text{s}$. Comparing to the bifurcation diagrams of the deterministic Ca^{2+} diffusion model given in Figs. 3 and 4, one can see that the stochastic channel dynamics modulate the Ca^{2+} oscillation behavior more at regions with bistable states in deterministic model. The stochastic noise typically destroys the multiple states. As a comparison between Figs. 4(d) and 9(b), if the bistable states are an oscillation with a fixed point in deterministic model, the stochastic model typically exhibits fluctuation around the fixed point. As a result, two oscillation regions are found with the increasing p at $D = 15\,\mu\text{m}^2/\text{s}$.

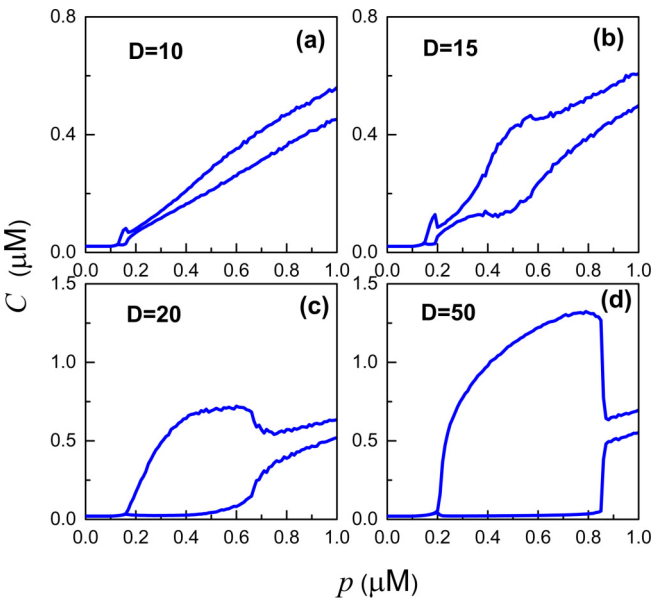

FIG. 9. Bifurcation diagrams of $\langle C\rangle$ against p for the noisy Ca^{2+} diffusion model at different D. In (a)–(d), $D = 10$, 15, 20, and $50\,\mu\text{m}^2/\text{s}$, respectively.

The bifurcation diagrams of $\langle C\rangle$ against D are shown in Figs. 10(a) and 10(b) for the noisy Ca^{2+} diffusion model with $N = 36$ at $p = 0.3$ and $0.2\,\mu$M, respectively. One can see in Fig. 10(b) that the wave failure can still be observed even with the stochastic channel dynamics. To show the robustness of wave failure in noisy Ca^{2+} diffusion model, we consider different channel number in Eq. (10). As examples, Figs. 10(c) and 10(d) plot the bifurcation diagrams at $N = 25$ and $p = 0.25\,\mu$M, and at $N = 15$ and $p = 0.45\,\mu$M, respectively. Our simulation results show that the wave failure is a robust behavior even in the noisy Ca^{2+} system.

IV. DISCUSSION

In this paper, we discuss the intracellular Ca^{2+} signaling with a two-dimensional model in which the channels are

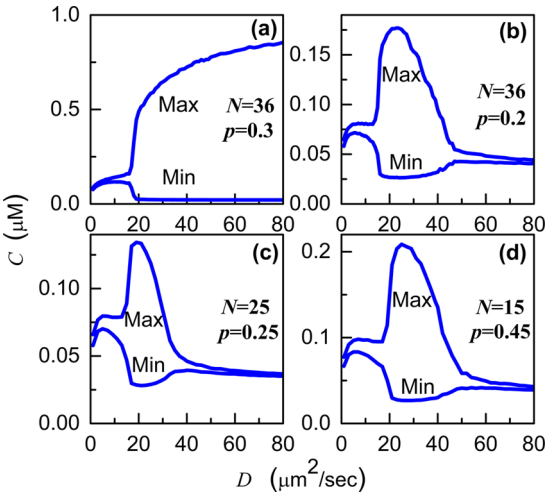

FIG. 10. Bifurcation diagrams of $\langle C \rangle$ against D for the noisy Ca^{2+} diffusion model at $p = 0.3\,\mu$M and $N = 36$ (a), $p = 0.2\,\mu$M and $N = 36$ (b), $p = 0.25\,\mu$M and $N = 25$ (c), and $p = 0.45\,\mu$M and $N = 15$ (d), respectively.

distributed in clusters. Thus, the Ca^{2+} diffusion media consists of a regular array of excitable regions embedded in a large passive region. The active regions with clustered channels can exhibit oscillation dynamics, while only with the pump dynamics and a small leakage term the passive region mainly acts as a sink to drive Ca^{2+} ions into cytosol from the ER pool. It has been shown that the clustered distribution of Ca^{2+} channels can generate various spatial Ca^{2+} signals, including localized puffs, stochastic backfiring, abortive waves, spiral waves, and globally salutatory or continuous waves [20,26–28]. By investigating the bifurcation diagrams of the global Ca^{2+} signals with varying Ca^{2+} diffusion coefficient and IP_3 stimulation, the wave failure at strong Ca^{2+} diffusion coefficient is discussed in detail in this paper.

The counterintuitive behavior of wave failure was first discussed in nonhomogenous media with a very simple model by Pando *et al.* in Ref. [34]. However, such an interesting phenomenon has recieved little attention by now. In this paper, we show that the wave failure can be observed in a more biologically realistic Ca^{2+} diffusion model. With the model, the propogation waves are found for D in the range of $10 \leqslant D \leqslant 45\,\mu m^2/s$, and the wave becomes failure at D larger than $45\,\mu m^2/s$ [Fig. 6(b)]. In cells, the diffusion coefficient of free Ca^{2+} ions is about $220\,\mu m^2/s$ [41]. In biological condition with various Ca^{2+} buffers, the effective diffusion coefficient is about 5–50 $\mu m^2/s$ [41], with a typical value of 20–30 $\mu m^2/s$ applied in many simulation models [21,26,27,29]. Thus, the wave failure occurs in our model with the effective diffusion coefficient of Ca^{2+} ions in biological range.

In our diffusing system, the media consists of excitable regions with the release dynamics of Ca^{2+} channels and passive region with the Ca^{2+} pump dynamics. In such an inhomogenous system, the intracellular Ca^{2+} ions are mainly released through IP_3R channels from ER in the active regions, and the passive region acts as a sink to drive Ca^{2+} ions back into ER. Thus, there is a net flux of Ca^{2+} ions from the active regions to passive region. With a large diffusion coefficent D, the Ca^{2+} ions will move more rapidly from the active regions to passive region. As a result, the Ca^{2+} diffusion plays a dual role in such inhomogeneous media. On the one hand, Ca^{2+} diffusion is necessary to generate wave propagation among excitable regions. On the other hand, Ca^{2+} diffusion removes Ca^{2+} ions from the excitable regions to destroy the Ca^{2+} oscillation. A proper interaction between the Ca^{2+} channel dynamics in excitable regions and the pump dynamics in passive region is necessary to support Ca^{2+} oscillation and wave propagation. The Ca^{2+} diffusion with a too large Ca^{2+} diffusion coefficient acts as a strong sink to remove lots of Ca^{2+} ions from the excitable regions, leading to the failure of Ca^{2+} waves. In our simulation, the wave failure can be observed with varying model paramters, including different channel flux rates, pump flux rates and the channel numbers in each cluster, either with determinsitc or stochastic channel dynamics. Thus, the wave failure is a robust behivor in the model.

Another interesting observation is the two oscillation regions with the increasing p, which occurs either with deterministic diffusion model or with stochastic channel model. The signal of IP_3 strength is typically encoded into Ca^{2+} signal by Ca^{2+} oscillation for cellular functions [1]. The two oscillation regions in p indicate that the Ca^{2+} signaling system may encode the IP_3 stimulus in separated pieces, rather than with only one continuous range.

Compared to the biological Ca^{2+} system, our model is still quite simple with two-dimensional space. During the release events, the Ca^{2+} concentration in ER is assumed to keep constant. Various Ca^{2+} buffers are ignored by simply considering an effective diffusion coefficient for free Ca^{2+} ions. Thus, the complex bifurcations may depend on some of the idealizations of the model, such as the specific IP_3R channel model. Nevertheless, the fact that the wave failure has been observed either in an abstract model by Pando *et al.* [19] or in a more biological realistic model in this paper indicates that the wave failure should be a general behavior in inhomogeneous diffusing systems.

As a prediction, the wave failure may occur in biological Ca^{2+} signaling systems. To test this hypothesis in experimental Ca^{2+} system, one has to modulate the effective diffusion coefficient of Ca^{2+} ions. As a fact, the Ca^{2+} buffers play a key role in affecting Ca^{2+} diffusional mobility. Immobile buffers can reduce the effective diffusion coefficient of Ca^{2+}, whereas mobile buffers can act as a shuttle to speed Ca^{2+} diffusion in the presence of immobile buffers [42]. Especially, the mobile buffers with fast on-rate, such as BAPTA and calretinin, can slow Ca^{2+} responses and promote globalization of spatially uniform Ca^{2+} signals [43,44]. We propose that one may discuss the Ca^{2+} responses in the presence of different concentrations of exogenous Ca^{2+} buffers to test the hypothesis of wave failure.

ACKNOWLEDGMENTS

We acknowledge support from the National Natural Science Foundation of China (Grants No. 11675134 and No. 11704318), the China Postdoctoral Science Foundation (Grant No. 2016M602071), and the 111 Project (Grant No. B16029).

[1] M. J. Berridge, M. D. Bootman, and P. Lipp, Nature **395**, 645 (1998).
[2] D. E. Clapham, Cell **131**, 1047 (2007).
[3] E. B. Ridgeway *et al.*, Proc. Natl. Acad. Sci. U.S.A. **74**, 623 (1977).
[4] R. Miledi, I. Parker, and G. Schalow, Nature **268**, 750 (1977).
[5] J. Lechleiter, S. Girard, E. Peralta, and D. Clapham, Science **252**, 123 (1991).
[6] I. Parker and Y. Yao, Proc. R. Soc. London B **246**, 269 (1991).
[7] N. Bazargani and D. Attwell, Nat. Neurosci. **19**, 182 (2016).
[8] H. Cheng, W. J. Lederer, and M. B. Cannell, Science **262**, 740 (1993).
[9] J. K. Foskett, C. White, K. H. Cheung, and D. O. D. Mak, Physiol. Rev. **87**, 593 (2007).
[10] H. Cheng and W. J. Lederere, Physiol. Rev. **88**, 1491 (2008).
[11] H. J. Rose, S. Dargan, J. W. Shuai, and I. Parker, Biophys. J. **91**, 4024 (2006).
[12] I. F. Smith and I. Parker, Proc. Natl. Acad. Sci. U.S.A. **106**, 6404 (2009).
[13] S. Rüdiger, Phys. Rep. **534**, 39 (2014).
[14] G. Dupont and J. Sneyd, Curr. Opin. Syst. Biol. **3**, 15 (2017)
[15] J. W. Shuai and P. Jung, Biophys. J. **83**, 87 (2002).
[16] J. W. Shuai and P. Jung, Phys Rev Lett. **88**, 068102 (2002).
[17] S. Rüdiger, J. W. Shuai, and I. M. Sokolov, Phys. Rev. Lett. **105**, 048103 (2010).
[18] K. Thurley and M. Falcke, Proc. Natl. Acad. Sci. U.S.A. **108**, 427 (2011).
[19] J. Sneyd, J. M. Han, L. Wang, J. Chen, X. Yang, A. Tanimura, M. J. Sanderson, V. Kirk, and D. I. Yule, Proc. Natl. Acad. Sci. U.S.A. **114**, 1456 (2017).
[20] S. P. Dawson, J. Keizer, and J. E. Pearson, Proc. Natl. Acad. Sci. U.S.A. **96**, 6060 (1999).
[21] S. Coombes and Y. Timofeeva, Phys. Rev. E **68**, 021915 (2003).
[22] J. W. Shuai, Y. D. Huang, and S. Rüdiger, Phys. Rev. E **81**, 041904 (2010).
[23] S. Rüdiger, P. Jung, and J. W. Shuai, PLoS Comput. Biol. **8**, e1002485 (2012).
[24] M. Rückl, I. Parker, J. S. Marchant, C. Nagaiah, F. W. Johenning, and S. Rüdiger, PLoS Comput. Biol. **11**, e1003965 (2015).
[25] P. Li, W. Wei, X. Cai, C. Soeller, M. B. Cannell, and A. V. Holden, Phil. Trans. R. Soc. A **368**, 3953 (2010).
[26] M. Falcke, M. Or-Guil, and M. Bär, Phys. Rev. Lett. **84**, 4753 (2000)
[27] M. Falcke, L. Tsimring, and H. Levine, Phys. Rev. E **62**, 2636 (2000)
[28] J.W. Shuai and P. Jung, Phys. Rev. E **67**, 031905 (2003).
[29] J. W. Shuai and P. Jung, Proc. Natl. Acad. Sci. U.S.A. **100**, 506 (2003).
[30] J. Sneyd, K. Tsaneva-Atanasova, D. I. Yule, J. L. Thompson, and T. J. Shuttleworth, Proc. Natl. Acad. Sci. U.S.A. **101**, 1392 (2004).
[31] X. L. Liao, P. Jung, and J. W. Shuai, Phys. Rev. E **79**, 041923 (2009).
[32] P. C. Bressloff, Physica D **155**, 83 (2001).
[33] Z. P. Kilpatrick, S. E. Folias, and P. C. Bressloff, SIAM J. Appl. Dyn. Sys. **7**, 161 (2008).
[34] B. Pando, J. E. Pearson, and S. P. Dawson, Phys. Rev. Lett. **91**, 258101 (2003).
[35] Y. Li and J. Rinzel, J. Theor. Biol. **166**, 461 (1994).
[36] G. W. De Young and J. Keizer, Proc. Natl. Acad. Sci. U.S.A. **89**, 9895 (1992).
[37] L. Ionescu, C. White, K. H. Cheung, J. W. Shuai, I. Parker, J. E. Pearson, J. K. Foskett, and D. O. Mak, J. Gen. Physiol. **130**, 631 (2007).
[38] J. W. Shuai, D. Yang, J. W. Pearson, and S. Ruediger, Chaos **19**, 037105 (2009).
[39] G. Ullah, D. O. Mak, and J. E. Pearson, J. Gen. Physiol. **140**, 159 (2012).
[40] B. A. Bicknell and G. J. Goodhill, Proc. Natl. Acad. Sci. U.S.A. **113**, E5288 (2016).
[41] N. L. Allbritton, T. Meyer, and L. Stryer, Science **258**, 1812 (1992).
[42] W. M. Roberts, J. Neurosci. **14**, 3246 (1994).
[43] S. L. Dargan and I. Parker, J. Physiol. **553**, 775 (2003).
[44] S. L. Dargan, B. Schwaller, and I. Parker, J. Physiol. **556**, 447 (2004).